

# Journal of Biomedical Optics

BiomedicalOptics.SPIEDigitalLibrary.org

## **Study on the validity of $3 \times 3$ Mueller matrix decomposition**

Yunfei Wang  
Yihong Guo  
Nan Zeng  
Dongsheng Chen  
Honghui He  
Hui Ma

# Study on the validity of $3 \times 3$ Mueller matrix decomposition

Yunfei Wang,<sup>a,†</sup> Yihong Guo,<sup>b,†</sup> Nan Zeng,<sup>a</sup> Dongsheng Chen,<sup>a</sup> Honghui He,<sup>a</sup> and Hui Ma<sup>a,\*</sup>

<sup>a</sup>Tsinghua University, Institute of Optical Imaging and Sensing, Graduate School at Shenzhen, Shenzhen Key Laboratory for Minimal Invasive Medical Technologies, Shenzhen 518055, China

<sup>b</sup>Peking University, Institute of Software, School of Electronic and Computer Science, Key Laboratory of High Confidence Software Technologies, Beijing 100084, China

**Abstract.** Using Monte Carlo simulations based on previously developed scattering models consisting of spherical and cylindrical scatterers imbedded in birefringent interstitial medium, we compare the polarization parameters extracted from the  $3 \times 3$  and  $4 \times 4$  Mueller matrix decomposition methods in forward and backward scattering directions. The results show that the parameters derived from the  $3 \times 3$  Mueller matrix decomposition are usually not the same as those from the  $4 \times 4$  Mueller matrix decomposition but display similar qualitative relations to changes in the microstructure of the sample, such as the density, size, and orientation distributions of the scatterers, and birefringence of the interstitial medium. The simulations are backed up by experiments when suitable samples are available. © The Authors. Published by SPIE under a Creative Commons Attribution 3.0 Unported License. Distribution or reproduction of this work in whole or in part requires full attribution of the original publication, including its DOI. [DOI: [10.1117/1.JBO.20.6.065003](https://doi.org/10.1117/1.JBO.20.6.065003)]

Keywords: polar decomposition; polarization; Mueller matrix.

Paper 150120R received Mar. 1, 2015; accepted for publication May 7, 2015; published online Jun. 3, 2015.

## 1 Introduction

A Mueller matrix contains rich information on the polarization properties of complex samples such as biological tissues.<sup>1,2</sup> In general, obtaining a Mueller matrix requires at least 16 polarization measurements involving both linear and circular polarization components. Since the 16 elements of a Mueller matrix are usually not explicitly linked to the characteristic microstructure of the sample, various decomposition methods have been proposed to relate the Mueller matrix to different mechanisms which affect the polarization of the scattered light.<sup>3–8</sup> For example, Lu and Chipman decompose a Mueller matrix into three contributions of known physics meanings: diattenuation, retardance, and depolarization.<sup>3</sup> Such a Mueller matrix polar decomposition technique has been used as an effective tool for quantitatively characterizing the polarization properties of pathological samples.<sup>9–12</sup> It has been found in some biomedical applications that the linear polarization properties are sufficient to identify samples. For example, Wang et al. used linear depolarization and linear retardance to distinguish *ex vivo* normal and cancerous gastric samples.<sup>13</sup> Since measurements of the last row and column of Mueller matrix elements need retardance modulations, which adds stricter requirements to bandwidths of the light sources and stability of the optical alignments, measuring only the linear polarization properties or the partial  $3 \times 3$  Mueller matrix without the last row and column will significantly simplify the polarization imaging system. In fact, the newly bioinspired CMOS polarization image sensor makes  $3 \times 3$  Mueller matrix imaging a routine practice in laboratories as well as in clinics.<sup>14</sup> However, the data processing algorithm for a  $4 \times 4$  Mueller matrix may not be applied directly to a  $3 \times 3$

Mueller matrix in general cases. Swami et al.<sup>15</sup> showed that for nondepolarizing media, various symmetry constraints on Mueller matrix elements can be used to obtain some of the  $4 \times 4$  Mueller matrix elements from the  $3 \times 3$  Mueller matrix. Swami et al.<sup>16</sup> presented a method based on the polar decomposition of a  $4 \times 4$  Mueller matrix to quantify independent polarization parameters: linear diattenuation, linear depolarization, linear retardance, and circular retardance using the nine elements of a  $3 \times 3$  Mueller matrix under the assumption that the depolarization of linear polarized light due to scattering is independent of the orientation angle of the incident linear polarization vector. Based on this decomposition method, Qi et al. designed a narrow-band  $3 \times 3$  Mueller matrix polarimetric imager in a rigid endoscope and used it for measuring the rat tissues. The results revealed that multispectral operation allows the detection of absorption features in addition to scattering-related contrast, which has shown the potential of the system in specific pathologies characterization.<sup>17</sup>

In previous studies, we have verified the validity of the sphere-cylinder scattering model<sup>18,19</sup> and sphere-cylinder-birefringence model<sup>20</sup> by comparison with experiments and other Monte Carlo (MC) simulations.<sup>21</sup> In this paper, we use the same models and MC simulations to generate forward scattering Mueller matrices and obtain two sets of polarization parameters using both  $3 \times 3$  and  $4 \times 4$  Mueller matrix decomposition methods. The simulated data are also backed up by experiments using samples containing polystyrene microspheres, well-aligned glass fibers and polyacrylamide. We examine, in detail, the quantitative relationship between the two sets of parameters and conclude that parameters derived by the  $3 \times 3$  and  $4 \times 4$  Mueller matrix decomposition are not equal to each other but vary in similar trends with the structural parameters of the scattering model. Images from a partial  $3 \times 3$  Mueller matrix decomposition demonstrate the resemblance to those from the full  $4 \times 4$  Mueller matrix decomposition.

\*Address all correspondence to: Hui Ma, E-mail: [mahui@tsinghua.edu.cn](mailto:mahui@tsinghua.edu.cn)

<sup>†</sup>These authors contributed equally to this work.

## 2 Material and Methods

### 2.1 Polarization Scattering Models and MC Simulation Program

The MC simulation program is used to track and record the polarization states of photons propagating in anisotropic media. The simulations are based on our polarization scattering models which approximate the microstructure of the sample, such as biological tissues, as a mixture of solid spherical and infinitely long cylindrical scatterers embedded in an interstitial medium (as shown in Fig. 1).<sup>18–20</sup> The parameters in the models are adjustable to simulate the microstructure and optical properties of different types of samples. For the scatterers, the variable parameters include the densities, sizes, complex refractive indices of the spheres, and cylinders, as well as the birefringence and angular distribution of the cylinders. For the interstitial medium, the variable parameters include the thickness, complex refractive index, birefringence, dichroism and optical activity coefficient. Corresponding to different samples, we can simplify these models to a sphere model, sphere-birefringence model (SBM), cylinder model, and sphere-cylinder model (SCM). Using a GPU-based simulation program, simulation of 10 million photons costs less than 1 min.

### 2.2 Polar Decomposition for 4 × 4 Mueller Matrix

For analyzing a 4 × 4 Mueller matrix, many decomposition methods have been developed, such as polar decomposition,<sup>3</sup> differential matrix of decomposition,<sup>22</sup> sum decomposition,<sup>23</sup> etc. A 4 × 4 Mueller matrix has the advantage of completely describing the polarization properties of any media by a minimum of 16 measurements involving both linearly and circularly polarized light. However, circular polarization measurements using waveplates usually lead to more system complexity and error fluctuations. In this paper, we choose the Lu-Chipman Mueller matrix polar decomposition (MMPD) method which decomposes a 4 × 4 Mueller matrix into the product of three factors with known physics meanings: diattenuation, retardance, and depolarization, as shown in Eq. (1).<sup>3</sup>

$$M = M_{\Delta} M_R M_D. \quad (1)$$

The matrices  $M_{\Delta}$ ,  $M_R$ , and  $M_D$  represent depolarization, retardance, and diattenuation, respectively. The value of diattenuation  $D$  is calculated from the  $M_D$  matrix as follows:<sup>3</sup>

$$D = \frac{1}{m_{11}} \sqrt{(m_{12}^2 + m_{13}^2 + m_{14}^2)}. \quad (2)$$

The depolarization coefficient  $\Delta$  is determined from the elements of matrix  $M_{\Delta}$ :<sup>3</sup>

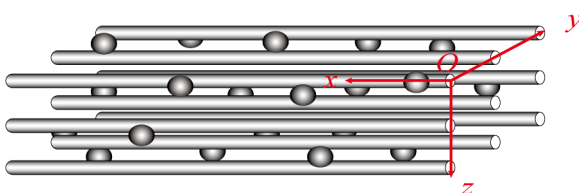


Fig. 1 Schematic of sphere-cylinder scattering model.

$$\Delta = 1 - \frac{|tr(M_{\Delta}) - 1|}{3}. \quad (3)$$

The last MMPD parameter, retardance  $R$ , is calculated from  $M_R$  and includes both the linear retardance  $\delta$  and the circular retardance  $\psi$ .<sup>3</sup>

$$R = \cos^{-1} \left[ \frac{tr(M_R)}{2} - 1 \right], \quad (4)$$

$$\delta = \cos^{-1} \left[ \sqrt{[M_R(2,2) + M_R(3,3)]^2 + [M_R(3,2) - M_R(2,3)]^2} - 1 \right], \quad (5)$$

$$\psi = \tan^{-1} \left[ \frac{M_R(3,2) - M_R(2,3)}{M_R(2,2) + M_R(3,3)} \right]. \quad (6)$$

### 2.3 Polar Decomposition for 3 × 3 Mueller Matrix

Matrix decomposition of the partial 3 × 3 Mueller matrix developed by Ghosh presents four independent linear polarization parameters, namely linear diattenuation, linear depolarization, linear retardance, and circular retardance.<sup>16</sup> A 3 × 3 partial Mueller matrix, by removing the last row and column of 4 × 4 Mueller matrix, can be obtained by linear polarization measurements using only polarizers without the waveplate. The simplification on the detection schedule is more suitable for some special clinic application, for example, the polarization endoscope.<sup>17</sup> However, the lack of a circular polarization component implies the possible loss of important information, such as the complex phase shift during scattering<sup>24</sup> and the discrepancies between corresponding parameters derived from the 4 × 4 and 3 × 3 Mueller matrix decomposition methods.

$$m = m_{\Delta} m_R m_D. \quad (7)$$

The matrices  $m_{\Delta}$ ,  $m_R$ , and  $m_D$  represent the linear polarization parameters of depolarization, retardance, and diattenuation. The value of linear diattenuation  $D$  is calculated from  $m_D$  matrix as follows:<sup>16</sup>

$$D = \frac{1}{m_{11}} \sqrt{(m_{12}^2 + m_{13}^2)}. \quad (8)$$

The inverse of  $m_D$  is multiplied with  $m$  to remove the diattenuation and the remaining matrix consists of depolarization and retardance.<sup>16</sup>

$$m' = m m_D^{-1} = m_{\Delta} m_R. \quad (9)$$

In order to obtain the values of linear depolarization, we construct a matrix  $m_{DR}$ :

$$m_{DR} = m'(m')^T, \quad (10)$$

$$\Delta = 1 - \sqrt{\lambda}, \quad (11)$$

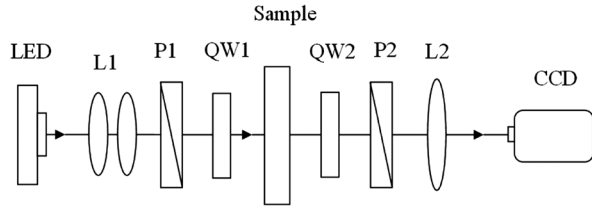


**Fig. 2** Schematic of forward scattering Mueller matrix measurement setup. LED: light source; L1,L2: lenses; P1,P2: polarizers; and QW1, QW2: quarter waveplates.

where  $\lambda$  is the larger one of the remaining two eigen values of the matrix  $m_{DR}$  except for the eigen value of unity after normalization.<sup>16</sup>

Then the retardance matrix  $m_R$  can be constructed by multiplying the inverse of  $m_\Delta$  with  $m'$ :<sup>16</sup>

$$m_R = m_\Delta^{-1} m', \quad (12)$$

$$\delta = \cos^{-1} \left[ \frac{\sqrt{[m_R(2,2) + m_R(3,3)]^2 + [m_R(3,2) - m_R(2,3)]^2}}{-1} \right], \quad (13)$$

$$M = \begin{pmatrix} m_{11} & m_{12} & m_{13} & m_{14} \\ m_{21} & m_{22} & m_{23} & m_{24} \\ m_{31} & m_{32} & m_{33} & m_{34} \\ m_{41} & m_{42} & m_{43} & m_{44} \end{pmatrix}$$

$$= \frac{1}{2} \begin{pmatrix} \text{HH} + \text{HV} + \text{VH} + \text{VV} & \text{HH} + \text{HV} - \text{VH} - \text{VV} & \text{PH} + \text{PV} - \text{MP} - \text{MM} & \text{RH} + \text{RV} - \text{LH} - \text{LV} \\ \text{HH} - \text{HV} + \text{VH} - \text{VV} & \text{HH} - \text{HV} - \text{VH} + \text{VV} & \text{PH} - \text{PV} - \text{MH} - \text{MV} & \text{RH} - \text{RV} - \text{LH} + \text{LV} \\ \text{HP} - \text{HM} + \text{VP} - \text{VM} & \text{HP} - \text{HM} - \text{VP} + \text{VM} & \text{PP} - \text{PM} - \text{MP} + \text{MM} & \text{RP} - \text{RM} - \text{LP} + \text{LM} \\ \text{VR} + \text{HR} - \text{LL} - \text{RL} & \text{VL} + \text{HR} - \text{HL} - \text{VR} & \text{ML} + \text{PR} - \text{PL} - \text{MR} & \text{RR} + \text{LL} - \text{LR} - \text{RL} \end{pmatrix}. \quad (15)$$

The first letter represents the input polarization state. The second letter represents the output polarization state. In experiments, we define a reference coordinate system with its  $x$  axis parallel to the optical platform and  $y$  axis perpendicular to it. The surface of the sample is set to the  $x$ - $y$  plane.

The anisotropic phantom sample contains polystyrene microspheres and well-aligned glass fibers as scatterers embedded in polyacrylamide (as shown in Fig. 3). The diameter and refractive index of the polystyrene microspheres are  $1\text{-}\mu\text{m}$  and 1.59, respectively. The glass fibers with a  $10\text{-}\mu\text{m}$  diameter and 1.547 refractive index are well aligned by winding them neatly around a metal frame and are then immersed in polyacrylamide

$$\psi = \frac{1}{2} \tan^{-1} \left[ \frac{m_R(2,3) - m_R(3,2)}{m_R(2,2) + m_R(3,3)} \right]. \quad (14)$$

## 2.4 Experimental Methods

The experiment setup for forward scattering Mueller matrix measurement is shown in Fig. 2. A 3W LED is used as the light source with its center wavelength of 650 nm. After beam expansion and collimation, the incident light passes through a set of linear polarizer and quarter waveplates to be modulated into six polarization states: horizontal linear (H), vertical linear (V), 45 deg linear (P), 135 deg linear (M), and right/left(R/L) circular. The scattering light from the samples is examined by the analyzer, which is also a set of quarter waveplates and linear polarizers, and is finally collected by a lens and recorded by a CCD (Q-imaging Retiga Exi, 12-bit). For each incident polarization state, six components of the forward scattering light are detected through the analyzer. The Mueller matrix is calculated from the 36 raw images according to Eq. (15):

whose birefringence can be varied with the application of an external force. The polyacrylamide is cut into a  $4\text{ cm} \times 2\text{ cm} \times 1\text{ cm}$  cuboid (4-cm length, 2-cm width, and 1-cm thickness). The refractive index of the polyacrylamide is 1.393 and stretching the polyacrylamide can generate a controllable birefringence which is linearly proportional to the stretched length along the direction of the force (the extraordinary axis of birefringence).<sup>25</sup> We record Mueller matrices of different samples and carry on polar decompositions on both the full  $4 \times 4$  and partial  $3 \times 3$  Mueller matrices to obtain two sets of polarization parameters for comparison. The experimental results are also compared with those from MC simulations. The parameters of the

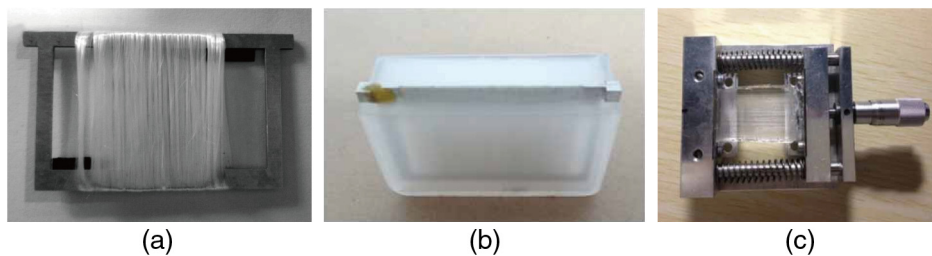


**Fig. 3** Schematic of phantom: (a) cylinder model; (b) sphere-cylinder model (SCM); and (c) sphere-cylinder birefringence model.

scatters and the interstitial medium are the same for both simulations and experiments.

### 3 Results and Discussion

We calibrate the experimental setup by measuring the Mueller matrix of some standard samples such as air and linear polarizers. The results show that the errors of the measured Mueller matrix are less than 5%. Then we start with a simple isotropic model with only spheres uniformly distributed in a homogeneous and isotropic medium. It is known that spherical scatterers contribute only to depolarization, not to diattenuation and retardance.<sup>26</sup> We apply  $4 \times 4$  and  $3 \times 3$  decomposition methods to the experimental and simulated Mueller matrices for the spheres with different scattering coefficients and sizes, as shown in Figs. 4(a)–4(c). Since the value of diattenuation remains at zero, we neglect it in the discussions. When using a  $4 \times 4$  or a  $3 \times 3$  decomposition method, both simulations and experiments show a similar tendency of the depolarization varying with the scattering coefficient and the scatterer's size. Quantitatively, the derived depolarization of spheres is larger for the  $3 \times 3$  decomposition. However, Figs. 4(a) and 4(b) also show that the  $3 \times 3$  decomposition results in an apparent retardance. This is an artifact because symmetry analysis does not support the existence of birefringence in such an isotropic system of spheres. The results from  $4 \times 4$  decomposition in Fig. 4(c) also show no clear signs of retardance.

For anisotropic samples, we can use a birefringent interstitial medium and the SBM. We compare the  $4 \times 4$  and  $3 \times 3$  decomposition data for both simulated and experimental results, as shown in Figs. 5(a) and 5(b). The simulated curves of depolarization and linear retardance as functions of birefringence indicate that linear retardance derived by both the  $4 \times 4$  and  $3 \times 3$

Mueller matrix decomposition methods are similar. The deviation is attributed to the abnormal linear retardance due to the  $3 \times 3$  Mueller matrix decomposition as discussed in the previous section. As for depolarization, it agrees with what we conclude in Fig. 4. Figure 5(b) is the experimental result when stretching the polyacrylamide to produce birefringence and also confirms the consistent trends of depolarization, retardance, and the corresponding explanations.

It has been found in previous works that cylindrical scatterers also produce retardance.<sup>18,19</sup> The properties of cylinders, such as density, diameter, and orientation, also influence the anisotropy of the media. Here, we set the cylinders perpendicular to the  $z$  axis and make the angle between the cylinder axis and  $x$  axis follow a Gaussian distribution described by its full width at half maximum (FWHM). Both the simulation results in Fig. 6(a) and experimental results in Fig. 6(b) show that the depolarization and linear retardance increase monotonously with the scattering coefficient for both  $3 \times 3$  and  $4 \times 4$  Mueller matrix decompositions. In experiments, the aligned cylindrical scatterers are glass fibers wound around a metal frame. We overlay several layers of the fibers to change the thickness of the sample, which is equivalent to changing the scattering coefficient of the cylinders. As shown in Figs. 6(c) and 6(d),  $\Delta$  and  $\delta$  from the two decomposition methods are usually different but follow similar relationships with the diameter of the cylinders. Figure 6(e) also shows that the linear retardance and depolarization derived from both the  $4 \times 4$  and  $3 \times 3$  Mueller matrix are usually different but follow the same trend. As the orientations of the cylinders become increasingly randomized, the system gets closer to isotropy. The  $3 \times 3$  Mueller matrix can produce nearly the same depolarization and linear retardance as the  $4 \times 4$  Mueller matrix if the cylinders

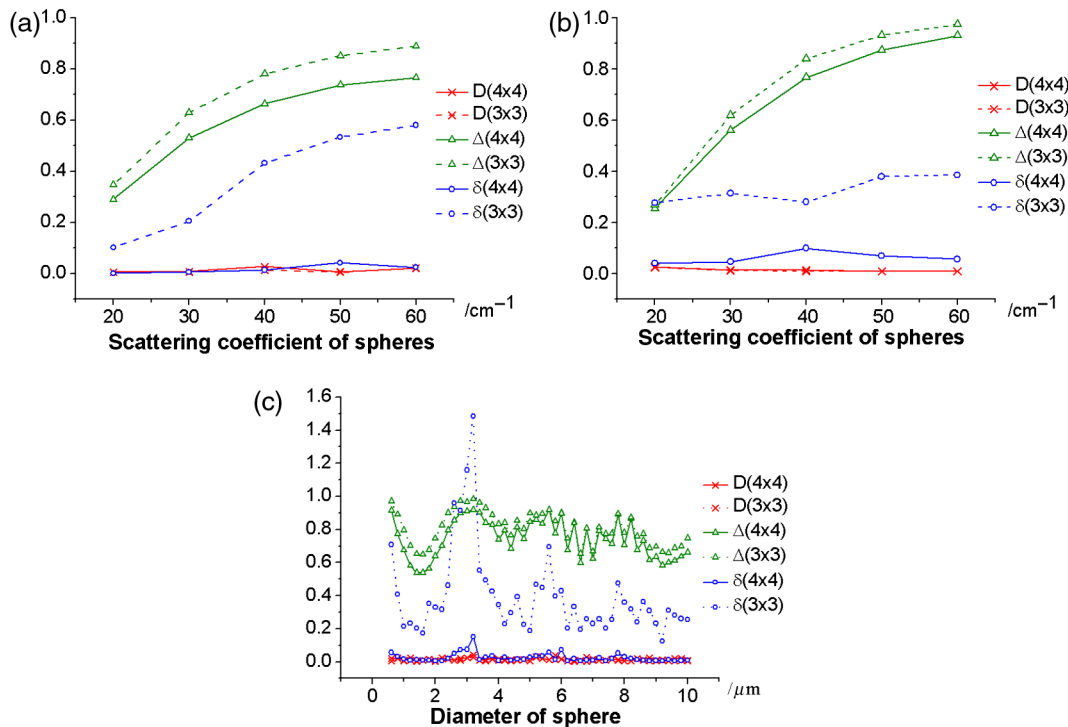


**Fig. 4** Mueller matrix polar decomposition results: (a) Monte Carlo (MC) simulation of different scattering coefficients, (b) experiments of different scattering coefficients, and (c) MC simulation of different diameters. In (a) and (b), the diameter of sphere is  $1 \mu\text{m}$ . In (c), the scattering coefficient of spheres is  $40 \text{ cm}^{-1}$ . For all of them, the refractive index is 1.59 for spheres and 1.33 for ambient medium.

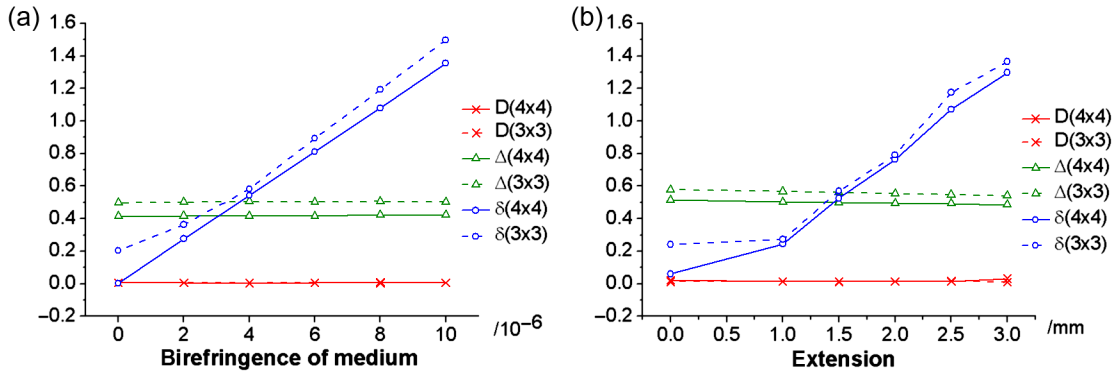


**Fig. 5** Mueller matrix polar decomposition results: (a) MC simulation and (b) experiments in forward direction. The sample of polyacrylamide is 4 cm × 2 cm × 1 cm with microspheres uniformly distributed in it. The refractive index is 1.393. Stretching produces variable linear birefringence. The scattering coefficients for both simulation and experiment are set to 30 cm<sup>-1</sup> with microspheres of 1 μm diameter and refractive index of 1.59.

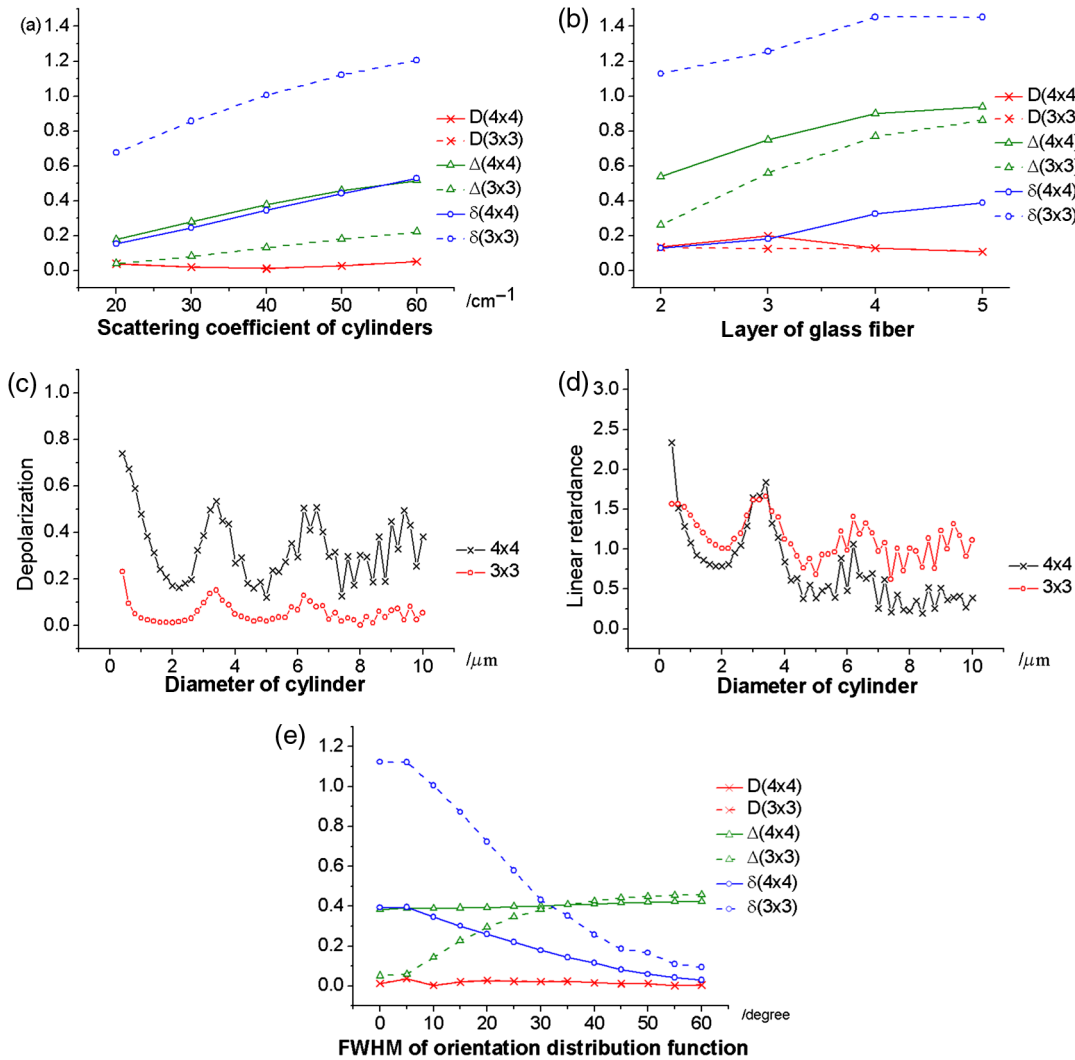


**Fig. 6** Mueller matrix polar decomposition results: (a) MC simulation on a layer of cylinders with fixed thickness and varying scattering coefficient and (b) experiment in forward direction on varying number of layers of glass fiber. (c) and (d) MC simulation on different sizes of cylinders. (e) MC simulation on different orientation angle of cylinders. In both simulation and experiment, the refractive index of cylinder is 1.547. The refractive index of surrounding medium is 1.33.

are totally disordered. In both simulations and experiments, the  $3 \times 3$  Mueller matrix produces higher retardance. But different from the case of spheres as scatterers, the cylindrical scatterers generate less depolarization. Considering only using the linear depolarization from the  $3 \times 3$  Mueller matrix, the decreased depolarization can be due to the weakened depolarization process for the incident linear polarization status parallel and perpendicular to the cylinders. For a  $3 \times 3$  Mueller matrix, cylinders with a good order corresponding to less depolarization also can be used to explain Fig. 6(e), where the depolarization value is sensitive to the FWHM of orientation distribution and apparently disordered cylinders depolarize light more. In short, for qualitative analysis, both decomposition methods show a similar regularity with the change of the anisotropy degree induced by cylindrical scatterers.

Furthermore, we mix the isotropic spherical scatterers with the anisotropic cylindrical scatterers to build the SCM whose anisotropy degree can be adjusted by changing the ratio between these two types of scatterers. Here, the orientation distribution of cylinders has a FWHM of 5 deg. Figures 7(a) and 7(b) demonstrate the results from a simulated forward scattering Mueller matrix with varying scattering coefficients of either spheres or cylinders. For both the  $4 \times 4$  and  $3 \times 3$  Mueller matrix decompositions, the magnitudes and their differences of depolarization and retardance increase as the proportion of the cylinders increases. The  $3 \times 3$  Mueller matrix always gives a smaller depolarization and bigger linear retardance. The results are consistent with what we conclude in Fig. 6(a). Meanwhile, in Fig. 7(b), the variation tendency of the depolarization curves is similar for  $3 \times 3$  and  $4 \times 4$  Mueller matrix decompositions, but

the retardance changes with the increasing spherical scattering coefficient are different. Linear retardance is smaller for the  $3 \times 3$  Mueller matrix but remains stable for the  $4 \times 4$  Mueller matrix. Both Figs. 7(a) and 7(b) support that larger cylinder-sphere ratios increase the quantitative difference between  $3 \times 3$  and  $4 \times 4$  Mueller matrix decompositions. In addition, the crossing of the depolarization curves in Fig. 7(b) can be explained as follows: the cylindrical scattering effect is dominant at the beginning, meaning a lower depolarization from a  $3 \times 3$  Mueller matrix similar with Fig. 6(a). But gradually, spherical scattering contributes more and more, then a higher depolarization can be generated from the  $3 \times 3$  Mueller matrix similar to Fig. 4(a). In brief, the comparison using forward MMPD indicates once again the feasibility of qualitative analysis and the difference of quantitative characterization using a  $3 \times 3$  Mueller matrix decomposition method.

We also carried on a similar analysis for backward scattering. Figures 7(c) and 7(d) correspond to the simulation results of SCM in the backward direction. We just change the detection direction and count the backscattered photons in the same simulation for the same scattering model with Figs. 7(a) and 7(b). It can be seen that the depolarization change with the scattering coefficient of cylinders in the media is different using backward MMPD from the forward case. In the backward condition, increasing the content of the cylinders has little influence on the depolarization and even causes a slight decrease for the  $3 \times 3$  Mueller matrix decomposition. But for the comparison between these two types of decomposition methods, the relationship between MMPD parameters and the scatterer change always has the same variation tendency. The backward

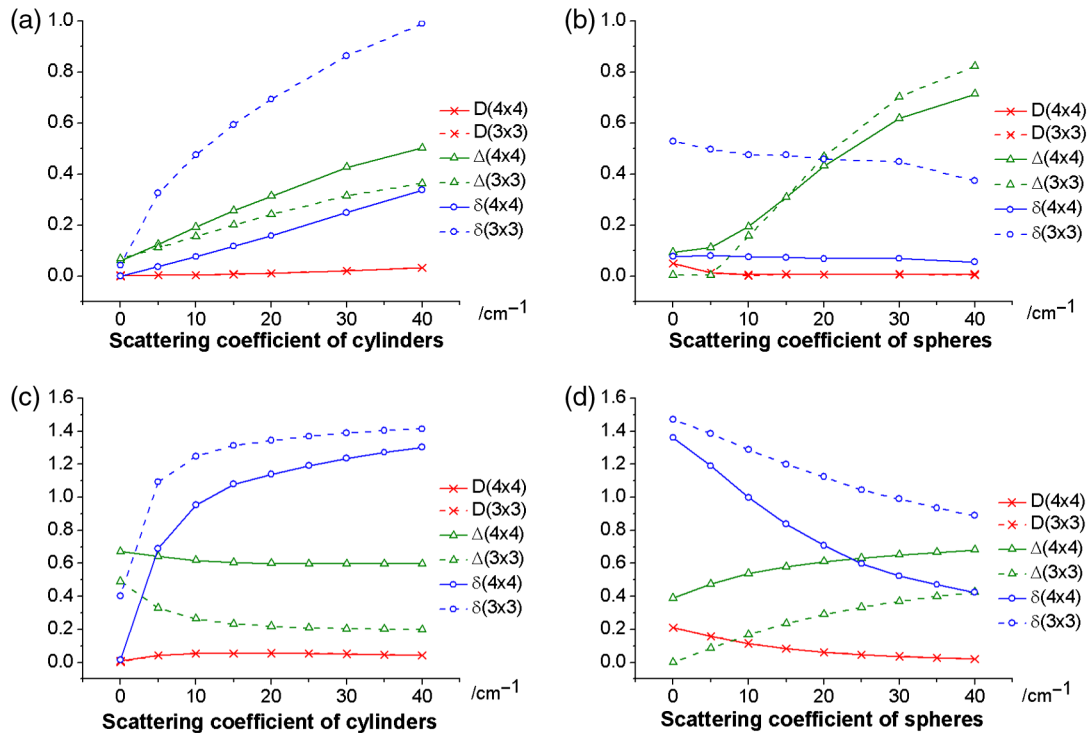


**Fig. 7** MC simulation on SCM: (a) and (b) forward direction detection; (c) and (d) backward direction detection. (a) and (c) the scattering coefficient of the spheres  $10 \text{ cm}^{-1}$  remains unchanged and increases the scattering coefficient of the cylinders. (b) and (d) the scattering coefficient of the cylinders  $10 \text{ cm}^{-1}$  remains unchanged and increases the scattering coefficient of spheres. For the sphere, its diameter is  $1 \mu\text{m}$  and refractive index is 1.59. For the cylinder, its diameter is  $10 \mu\text{m}$  and refractive index is 1.547.

simulation results confirm again the feasibility of the  $3 \times 3$  Mueller matrix decomposition method applied in qualitative analysis and the deviation for quantitative characterization.

## 4 Conclusion

Using MC simulations based on various models composed of spherical scatterers, cylindrical scatterers, and birefringent interstitial medium, we compare the polarization parameters extracted, respectively, with the  $4 \times 4$  and  $3 \times 3$  Mueller matrix decompositions in the forward scattering direction. The simulations are backed up by experiments when suitable samples are available. The simulated and the experimental results show that the depolarization and linear retardance obtained from the  $3 \times 3$  and  $4 \times 4$  Mueller matrix decompositions are usually not the same quantitatively, but display similar qualitative relations to changes in the microstructure of the sample, such as the density, size, and orientation distributions of the scatterers and birefringence of the interstitial medium. For depolarization, the  $3 \times 3$  Mueller matrix decomposition results in bigger contributions from the spheres and a smaller contribution from the cylinders. For retardance, both decomposition methods can present the phase retardance, respectively, due to two types of anisotropy sources in the tissue models: birefringence in the ambient medium and the cylindrical scatterers. Compared with birefringence, the retardance deviation due to cylinders using the  $3 \times 3$  Mueller matrix is more apparent. Additionally, it should be noted that the decomposition of the  $3 \times 3$  Mueller matrix for spheres can generate a singularly higher linear retardance, which can be confused with the real anisotropic microstructure or optical birefringence. We also carried on the above comparison of these two decomposition methods in the backward scattering detection and obtained similar conclusions. Therefore, the parameters for the  $3 \times 3$  Mueller matrix decomposition method follow the same qualitative trends as the corresponding results for the  $4 \times 4$  Mueller matrix decomposition method, although quantitatively, the two sets of parameters could be significantly different. Images of the corresponding  $3 \times 3$  and  $4 \times 4$  decomposition parameters should display similar patterns but different contrasts.

## Acknowledgments

This work has been supported by National Natural Science Foundation of China (NSFC). Grants No. 11174178, 11374179, 61205199, 41475125.

## References

1. T. Novikova et al., "The origins of polarimetric image contrast between healthy and cancerous human colon tissue," *Appl. Phys. Lett.* **102**(24), 241103 (2013).
2. Y. A. Ushenko et al., "Mueller-matrix diagnostics of optical properties of polycrystalline networks of human blood plasma," *Opt. Spectrosc.* **112**(6), 884–892 (2012).
3. S. Y. Lu and R. A. Chipman, "Interpretation of Mueller matrices based on polar decomposition," *J. Opt. Soc. Am. A* **13**(5), 1106–1113 (1996).
4. N. Ortega-Quijano and J. L. Arce-Diego, "Mueller matrix differential decomposition," *Opt. Lett.* **36**(10), 1942–1944 (2011).

5. M. Sun et al., "Characterizing the microstructures of biological tissues using Mueller matrix and transformed polarization parameters," *Biomed. Opt. Express* **5**(12), 4223–4234 (2014).
6. S. Manhas et al., "Mueller matrix approach for determination of optical rotation in chiral turbid media in backscattering geometry," *Opt. Express* **14**(1), 190–202 (2006).
7. H. He et al., "Two-dimensional and surface backscattering Mueller matrices of anisotropic sphere-cylinder scattering media: a quantitative study of influence from fibrous scatterers," *J. Biomed. Opt.* **18**(4), 046002 (2013).
8. F. Boulvert et al., "Decomposition algorithm of an experimental Mueller matrix," *Opt. Commun.* **282**(5), 692–704 (2009).
9. J. Chung et al., "Use of polar decomposition for the diagnosis of oral precancer," *Appl. Opt.* **46**(15), 3038–3045 (2007).
10. P. Shukla and A. Pradhan, "Mueller decomposition images for cervical tissue: Potential for discriminating normal and dysplastic states," *Opt. Express* **17**(3), 1600–1609 (2009).
11. P. G. Ellingsen et al., "Quantitative characterization of articular cartilage using Mueller matrix imaging and multiphoton microscopy," *J. Biomed. Opt.* **16**(11), 116002 (2011).
12. X. Wang, J. Lai, and Z. Li, "Polarization studies for backscattering of RBC suspensions based on Mueller matrix decomposition," *Opt. Express* **20**(18), 20771–20782 (2012).
13. W. Wang et al., "Roles of linear and circular polarization properties and effect of wavelength choice on differentiation between ex vivo normal and cancerous gastric samples," *J. Biomed. Opt.* **19**(4), 046020 (2014).
14. M. Zhang et al., "Bioinspired focal-plane polarization image sensor design: from application to implementation," *Proc. IEEE* **102**(10), 1435–1449 (2014).
15. M. K. Swami, H. S. Patel, and P. K. Gupta, "Conversion of  $3 \times 3$  Mueller matrix to  $4 \times 4$  Mueller matrix for non-depolarizing samples," *Opt. Commun.* **286**, 18–22 (2013).
16. M. K. Swami et al., "Polar decomposition of  $3 \times 3$  Mueller matrix: a tool for quantitative tissue polarimetry," *Opt. Express* **14**(20), 9324–9337 (2006).
17. J. Qi et al., "Narrow band  $3 \times 3$  Mueller polarimetric endoscopy," *Biomed. Opt. Express* **4**(11), 2433–2449 (2013).
18. H. He et al., "Two-dimensional backscattering Mueller matrix of sphere-cylinder scattering medium," *Opt. Lett.* **35**(14), 2323–2325 (2010).
19. T. Yun et al., "Monte Carlo simulation of polarized photon scattering in anisotropic media," *Opt. Express* **17**(19), 16590–16602 (2009).
20. E. Du et al., "Two-dimensional backscattering Mueller matrix of sphere-cylinder birefringence media," *J. Biomed. Opt.* **17**(12), 126016 (2012).
21. X. Wang and L. V. Wang, "Propagation of polarized light in birefringent turbid media: a Monte Carlo study," *J. Biomed. Opt.* **7**(3), 279–290 (2002).
22. R. Ossikovski, "Differential matrix formalism for depolarizing anisotropic media," *Opt. Lett.* **36**(12), 2330–2332 (2011).
23. H. Arwin et al., "Sum decomposition of Mueller-matrix images and spectra of beetle cuticles," *Opt. Express* **23**(3), 1951–1966 (2015).
24. B. Kunnen et al., "Application of circularly polarized light for non-invasive diagnosis of cancerous tissues and turbid tissue-like scattering media," *J. Biophotonics* **8**(4), 317–323 (2015).
25. M. F. G. Wood, X. Guo, and I. A. Vitkin, "Polarized light propagation in multiply scattering media exhibiting both linear birefringence and optical activity: Monte Carlo model and experimental methodology," *J. Biomed. Opt.* **12**(1), 014029 (2007).
26. Y. Guo et al., "A study on forward scattering Mueller matrix decomposition in anisotropic medium," *Opt. Express* **21**(15), 18361–18370 (2013).

Biographies for the authors are not available.